

September 20, 2018

Dilepton Radiation in Heavy-Ion Collisions at Small Transverse Momentum

Mariola Klusek-Gawenda,^{1,*} Ralf Rapp,^{2,†}
Wolfgang Schäfer,^{1,‡} and Antoni Szczurek^{§1,¶}

¹*Institute of Nuclear Physics Polish Academy of Sciences,
Radzikowskiego 152, PL-31-342 Kraków, Poland*

²*Cyclotron Institute and Department of Physics and Astronomy,
Texas A&M University, College Station, TX 77843-3366, USA*

Abstract

We study the invariant-mass distributions of dileptons produced in ultrarelativistic heavy-ion collisions at very low pair transverse momenta, $P_T \leq 0.15$ GeV. Specifically, we investigate the interplay of thermal radiation with initial photon annihilation processes, $\gamma\gamma \rightarrow l^+l^-$, triggered by the coherent electromagnetic fields of the incoming nuclei. For the thermal radiation, we employ the emission from the QGP and hadronic phases with in-medium vector spectral functions which describes the inclusive excess radiation observed over a wide range of collision energies. For the coherent photon fusion processes, whose spectrum is much softer than for thermal radiation, we employ initial fluxes from the Fourier transform of charge distributions of the colliding nuclei in the equivalent-photon approximation. We first verify that the combination of photon fusion, thermal radiation and final-state hadron decays gives a fair description of the low- P_T dilepton mass spectra as recently measured by the STAR collaboration in $\sqrt{s_{NN}}=200$ GeV Au+Au collisions for different centrality classes, including experimental acceptance cuts. The coherent contribution dominates in peripheral collisions, while thermal radiation shows a markedly stronger increase with centrality. We perform similar calculations at lower collision energies ($\sqrt{s_{NN}}=17.3$ GeV) and compare to the acceptance-corrected dimuon excess spectra measured by the NA60 experiment at the CERN SPS; here, the contribution from photoproduction is subleading. We also provide predictions for the ALICE experiment at the LHC; the pertinent excitation function from SPS to LHC energies reveals a nontrivial interplay of photoproduction and thermal radiation.

[§] Also at *Faculty of Mathematics and Natural Sciences, University of Rzeszów, Pigońia 1, PL-35-310 Rzeszów, Poland.*

*Electronic address: Mariola.Klusek@ifj.edu.pl

†Electronic address: rapp@comp.tamu.edu

‡Electronic address: Wolfgang.Schafer@ifj.edu.pl

¶Electronic address: Antoni.Szczurek@ifj.edu.pl

I. INTRODUCTION

Dilepton production in ultra-relativistic heavy-ion collisions (URHICs) has a long history as a probe of the hot QCD medium produced in these collisions [1, 2]. To date, the observed excess radiation over final-state hadron decays has been firmly established as thermal radiation from the interacting fireball [3, 4]. In the low-mass region, at invariant mass $M \lesssim 1$ GeV, hadronic radiation dominates revealing the melting of the ρ resonance [5], which indicates a transition to partonic degrees of freedom and is consistent with chiral symmetry restoration [6]. In the intermediate-mass region, quark-gluon plasma (QGP) radiation dominates [7, 8], opening the possibility for direct measurements of its temperature [9].

On the other hand, recent measurement of dileptons in ultraperipheral heavy-ion collisions (UPCs) [10–12], where the incoming nuclei do not touch and thus no fireball is created, have also revealed a substantial amount of dilepton radiation at both low and intermediate masses. This radiation is characterized by a very soft slope in pair transverse momentum, P_T , much steeper than for thermal radiation emitted from strongly interacting fireballs. A good description of the ultraperipheral dilepton data can be achieved with photon fusion reactions using realistic fluxes generated by the electromagnetic (EM) field of the highly relativistic incoming nuclei [13]. The coherent EM fields are expected to also give a contribution in impact parameter configurations where the two ions collide.

The question then arises how the interplay of these two processes works out in peripheral heavy-ion collisions, where thermal radiation is much suppressed compared to central collisions while the coherent photon emission is still appreciable. Recently, two of us have shown that J/ψ photoproduction in UPCs gives a significant contribution to the low- P_T production yield in semi-central collisions at the LHC [14], in agreement with the ALICE results for different centralities [15]. Similar findings have been reported in Ref. [16]. Recently, the STAR collaboration released new data for low- P_T e^+e^- production in 200 GeV Au+Au and U+U collisions over a large range of invariant mass and for different centralities [17]. In that work, initial model comparisons were conducted using contributions from thermal radiation [9] plus hadronic final-state decays plus photon fusion contributions from two different approaches [18, 19]. The general trend was that photon fusion processes dominate, and can explain, the low- P_T yield ($P_T < 0.15$ GeV) for peripheral collisions, although significant differences in the predicted yields are present. On the other hand, thermal radiation plus the hadronic decay “cocktail” increase much more rapidly with centrality and dominate the yield for $P_T > 0.2$ GeV at all centralities. A recent transport calculation [20] confirmed that hadronic sources (thermal emission plus cocktail) cannot explain the low- P_T excess observed by the STAR in peripheral Au-Au collisions. No photoproduction processes were considered in their study.

In the present paper we follow up on the above question by combining thermal radiation with photon fusion processes for low- P_T dilepton production. Quantitatively disentangling the two contributions in this regime provides important tests for either one, especially if systematic centrality and collision energy dependences can be established. After benchmarking our combined results against the STAR data at 200 GeV, we therefore expand our analysis to both lower and higher energies. For the former, we focus on In-In collisions at SPS energy ($\sqrt{s_{NN}}=17.3$ GeV) where we can test our predictions against the high-precision NA60 data [4, 21]; in fact, a low- P_T excess was observed in these data which has not been fully explained to date.

The paper is organized as follows. In Sec. II we briefly review the mechanisms for coherent photon fusion (Sec. II A) and thermal radiation (Sec. II B). In Sec. III we apply them to low- P_T dilepton invariant-mass spectra as measured at RHIC (Sec. III A) and the SPS (Sec. III B), make predictions for the LHC (Sec. III B), and compute an excitation function (Sec. III D). In Sec IV we conclude.

II. DILEPTON SOURCES

In this section we recall the main ingredients to the two main dilepton sources considered in this work, *i.e.*, the coherent initial photon fusion reactions in Sec. II A and thermal radiation in Sec. II B.

A. Initial Photon-Photon Fusion Mechanism

The main ingredient for the photon-photon fusion mechanism is the Weizsäcker-Williams flux of photons for an ion of charge Z moving along impact parameter \mathbf{b} ($b = |\mathbf{b}|$) with the Lorentz-boost parameter γ . With the nuclear charge form factor F_{em} as an input the flux can be calculated as [22, 23]

$$N(\omega, b) = \frac{Z^2 \alpha_{\text{EM}}}{\pi^2} \left| \int_0^\infty dq_T \frac{q_T^2 F_{\text{em}}(q_T^2 + \frac{\omega^2}{\gamma^2})}{q_T^2 + \frac{\omega^2}{\gamma^2}} J_1(bq_T) \right|^2, \quad (2.1)$$

where J_1 is a Bessel function. We calculate the formfactor from the Fourier transform of the nuclear charge density, for which parameterizations are available in Ref. [24].

The differential cross section for dilepton (l^+l^-) production via $\gamma\gamma$ fusion at fixed impact parameter \mathbf{b} of a nucleus nucleus collision can then be written as

$$\frac{d\sigma_{ll}}{d\tilde{\xi} d^2\mathbf{b}} = \int d^2\mathbf{b}_1 d^2\mathbf{b}_2 \delta^{(2)}(\mathbf{b} - \mathbf{b}_1 - \mathbf{b}_2) N(\omega_1, b_1) N(\omega_2, b_2) \frac{d\sigma(\gamma\gamma \rightarrow l^+l^-; \hat{s})}{d(-\hat{t})}, \quad (2.2)$$

where the phase space element is $d\tilde{\xi} = dy_+ dy_- dp_T^2$. Here, y_\pm , p_T and m_l are the single-lepton rapidities, transverse momentum and mass, respectively, and

$$\omega_1 = \frac{\sqrt{p_T^2 + m_l^2}}{2} (e^{y_+} + e^{y_-}), \quad \omega_2 = \frac{\sqrt{p_T^2 + m_l^2}}{2} (e^{-y_+} + e^{-y_-}), \quad \hat{s} = 4\omega_1\omega_2. \quad (2.3)$$

As can be seen from Eq.(2.1), the transverse momenta, q_T , of the photons have been integrated out, and dileptons are produced back-to-back in the transverse plane, *i.e.*, the transverse momentum P_T of the pair is neglected.

In UPCs the incoming nuclei do not touch, *i.e.*, no strong interactions occur between them. In this case one usually imposes the constraint $b > 2R_A$ when integrating over impact parameter $b = |\mathbf{b}|$. Here we lift this restriction allowing the nuclei to collide. Then the final state will no longer contain the intact nuclei but the dileptons will be produced on top of the hadronic nuclear event characterized by an impact parameter \mathbf{b} (or range thereof). Note that even for overlapping nuclei, $b < 2R_A$, leptons are predominantly produced outside the overlap region, for $b_{1,2} > R_A$. This situation is very different from

the photoproduction heavy vector mesons [14] which tend to be produced “inside” of one of the nuclei.

Here we are interested in the dependence on centrality. The mass-differential dilepton yield from coherent photons in a centrality class \mathcal{C} corresponding to an impact parameter range of $[b_{\min}, b_{\max}]$ is given by

$$\frac{dN_{ll}[\mathcal{C}]}{dM} = \frac{1}{f_{\mathcal{C}} \cdot \sigma_{AA}^{\text{in}}} \int_{b_{\min}}^{b_{\max}} db \int d\xi \delta(M - 2\sqrt{\omega_1 \omega_2}) \left. \frac{d\sigma_{ll}}{d\xi db} \right|_{\text{cuts}}, \quad (2.4)$$

where we have indicated kinematic cuts on single-lepton variables as applied in experiment, and $f_{\mathcal{C}}$ is the fraction of inelastic hadronic events contained in the centrality class \mathcal{C} ,

$$f_{\mathcal{C}} = \frac{1}{\sigma_{AA}^{\text{in}}} \int_{b_{\min}}^{b_{\max}} db \frac{d\sigma_{AA}^{\text{in}}}{db}. \quad (2.5)$$

We determine $[b_{\min}, b_{\max}]$ and σ_{AA}^{in} by using the optical Glauber model as

$$\frac{d\sigma_{AA}^{\text{in}}}{db} = 2\pi b (1 - e^{-\sigma_{NN}^{\text{in}} T_{AA}(b)}). \quad (2.6)$$

The nuclear thickness function, $T_{AA}(b)$, is obtained from the convolution of nuclear density distributions for which we use standard Woods-Saxon profiles, $n_A(r)$,

$$T_{AA}(b) = \int d^3\vec{r}_1 d^3\vec{r}_2 \delta^{(2)}(\mathbf{b} - \mathbf{r}_{1\perp} - \mathbf{r}_{2\perp}) n_A(r_1) n_A(r_2). \quad (2.7)$$

B. Thermal Dileptons

Thermal dilepton radiation in URHICs is based on the idea that the abundant production of hadrons, together with strong re-interactions, leads to the formation of a locally equilibrated medium whose expansion can be described by relativistic hydrodynamics. This idea is by now well established, on the one hand by the success of hydrodynamic modelling in reproducing the transverse-momentum spectra of the produced hadrons [25–27], and, on the other hand, by the observation and theoretical description of dilepton radiation that goes well beyond the final-state decays of the produced hadrons [3, 4, 9, 28]. The basic equation to compute dilepton invariant-mass spectra involves an integration of the 8-differential emission rate over the space-time evolution of the expanding fireball,

$$\frac{dN_{ll}}{dM} = \int d^4x \frac{M d^3P}{P_0} \frac{dN_{ll}}{d^4x d^4P}. \quad (2.8)$$

where (P_0, \vec{P}) and $M = \sqrt{P_0^2 - P^2}$ are the 4-vector ($P = |\vec{P}|$) and invariant mass of the lepton pair, respectively. The thermal emission rate can be expressed as

$$\frac{dN_{ll}}{d^4x d^4P} = -\frac{\alpha_{\text{EM}}^2 L(M)}{\pi^3 M^2} f^B(P_0; T) \text{Im} \Pi_{\text{EM}}(M, P; \mu_B, T), \quad (2.9)$$

in terms of the Bose distribution function, f^B , and the EM spectral function, $\text{Im} \Pi_{\text{EM}}$, depending on the local temperature, T , and baryon chemical potential, μ_B , of the medium

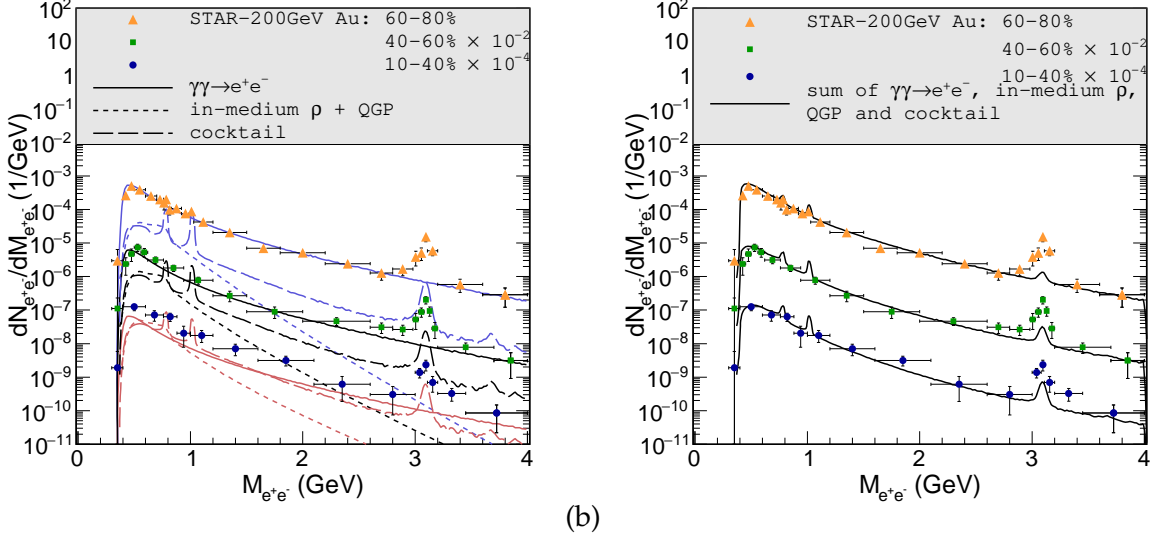


FIG. 1: (a) Dielectron invariant-mass spectra for pair $P_T < 0.15$ GeV in Au+Au ($\sqrt{s_{NN}}=200$ GeV) collisions for three centrality classes calculated (including experimental acceptance cuts, $p_T > 0.2$ GeV, $|\eta_e| < 1$ and $|y_{e^+e^-}| < 1$) for $\gamma\gamma$ fusion (solid lines), thermal radiation (dotted lines) and the hadronic cocktail (dashed lines). (b) Comparison of the total sum (solid lines) to STAR data [17].

($L(M)$ is a lepton phase-space factor which approaches one for $M \gg m_l$). The fireball medium generally goes through both QGP and hadronic phases; for the respective spectral functions we employ in-medium quark-antiquark annihilation constrained by lattice-QCD [28] and in-medium vector spectral functions in the hadronic sector [29]; the vector meson resonances strongly broaden in the medium and essentially melt at temperatures close to the pseudocritical one, providing a nearly smooth transition to the QGP rates. Different centrality classes for different colliding systems are characterized by the measured hadron multiplicities and appropriate initial conditions for the fireball. Its expansion is modelled by a simple volume parameterization guided by hydrodynamic models, and the underlying equation-of-state is based on $\mu_B=0$ lattice-QCD results for the QGP smoothly matched to a hadron resonance gas [9]. This approach is consistent with available dilepton data from SIS [30] via SPS [21, 31] to RHIC [32–34] energies.

III. LOW- P_T DILEPTON INVARIANT-MASS SPECTRA

We are now in position to combine the two sources described above and compare their sum to low- P_T measurements at RHIC (III A) and SPS (III B) and make predictions for the LHC (III C) and their excitation function (III D).

A. Au-Au Collisions at RHIC

In Fig. 1 we show dielectron invariant-mass spectra for small pair $P_T < 0.15$ GeV and three different centrality classes as selected in the STAR data: peripheral (60-80%), semi-peripheral (40-60%) and semi-central (10-40%) collisions. We also include the ex-

perimental acceptance cuts on the single-lepton tracks as applied by STAR, and take the cocktail contribution as provided by STAR [17] representing the final-state decays of the produced hadrons. In peripheral collisions the photon-photon contribution dominates while in semi-central collisions all three contributions are of similar magnitude. Their sum yields a rather good agreement with the STAR data, except for the J/ψ peak region. Our calculations only contain incoherent J/ψ production, from binary nucleon-nucleon collisions; we conjecture that the missing contribution is due to a coherent contribution discussed, *e.g.*, in Ref. [14], which we do not further pursue here, as our focus is on the interplay with thermal radiation.

B. In+In Collisions at the SPS

After benchmarking our approach with the STAR data, we now turn to the high-precision NA60 data from In-In ($\sqrt{s_{NN}}=17.3$ GeV) collisions at the SPS, for which no calculations of the coherent contribution are available to our knowledge. In addition, the dimuon P_T spectra of the NA60 collaboration show a distinct hint for an enhancement at very low P_T in various mass bins up to $M \simeq 1$ GeV that could not fully be explained by calculations of thermal radiation [4, 21].

In Fig. 2 we show the results of our calculations for thermal radiation and the coherent $\gamma\gamma$ mechanism for minimum bias (MB) In-In collisions, in comparison to the acceptance corrected NA60 excess data (from which the cocktail has also been subtracted). Unlike for RHIC energies the $\gamma\gamma$ contribution is rather small and only plays some role at small dimuon invariant masses where the NA60 data run out of precision.

C. Pb+Pb Collisions at the LHC

The rather different relative importance of low- P_T dilepton emission from coherent $\gamma\gamma$ and thermal radiation sources found at RHIC and SPS energies calls for their calculation at LHC energies. This is shown in Fig. 3 where we compare our predictions for the two sources for Pb+Pb collisions at $\sqrt{s_{NN}}=5.02$ TeV for the same centrality classes and single-lepton acceptance cuts as for our RHIC calculations above. Compared to the latter, the picture is qualitatively similar, although the strength of thermal contribution is relatively stronger, especially in semi-peripheral and central collisions where it is comparable and even larger, respectively, than the $\gamma\gamma$ yield at low mass.

D. Excitation Function

The results reported for the three different collision energies at the SPS, RHIC and the LHC in the previous three sections are now generalized into a systematic excitation function. In Fig. 4 we show the invariant-mass integrated low- P_T (<0.15 GeV) dilepton yields for the $\gamma\gamma$ and thermal components as a function of collision energy for the 3 centralities as used at RHIC and the LHC above, and including the same single-electron acceptance cuts. The photoproduction yields can be straightforwardly obtained from a direct calculation. For the thermal radiation, this would be much more involved. Instead we make use of the power-law like N_{ch} dependence of thermal radiation [28] together

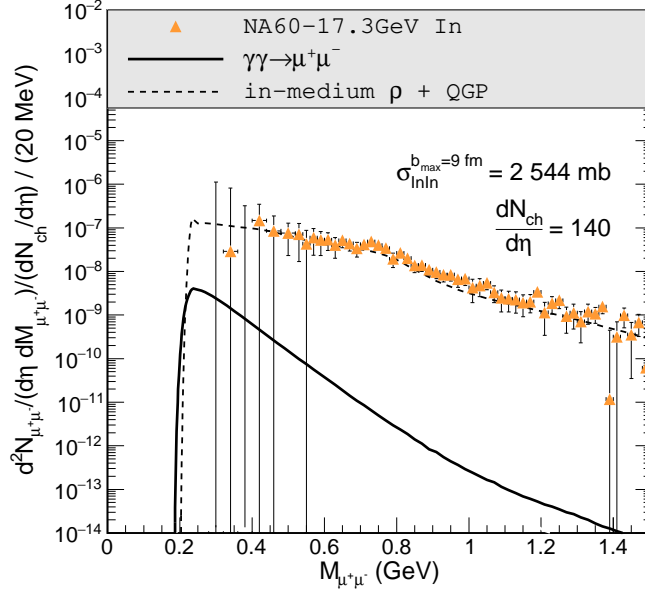


FIG. 2: Low- P_T (<0.2 GeV) acceptance-corrected dimuon invariant mass excess spectra in the rapidity range $3.3 < Y_{\mu^+\mu^-, LAB} < 4.2$ for MB In+In ($\sqrt{s_{NN}}=17.3$ GeV) collisions at the SPS. Calculations for coherent $\gamma\gamma$ fusion (solid line) and thermal radiation (dashed line) are compared to NA60 data [4, 21].

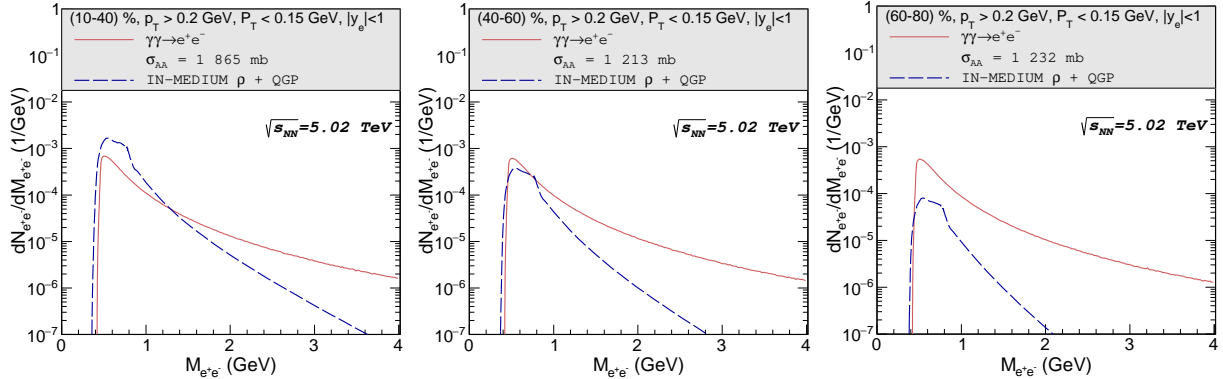


FIG. 3: Our predictions for low- P_T dilepton radiation in Pb+Pb ($\sqrt{s_{NN}}=5.02$ TeV) collisions from coherent $\gamma\gamma$ fusion (solid lines) and thermal radiation (dashed lines) for three centrality classes and acceptance cuts as specified in the figures.

with a power-law behavior of dN_{ch}/dy on collision energy [35] with the ansatz for $N_{ee}^{th} = N_0 s^\beta$. We then fit the two parameters, N_0 and β , independently for each of the three centrality classes considered above, including the experimental acceptance cuts.

The $\gamma\gamma$ fusion yield rises rather strongly in the tens of GeV collision energy regime, followed by a saturation above $\sqrt{s_{NN}} = 100$ GeV, while thermal radiation shows a much more gradual increase, cf. Fig. 4. The latter therefore dominates above the former at low energies, $\sqrt{s_{NN}} \lesssim 20$ GeV (as found in Sec. III B) at all centralities, and then increasingly

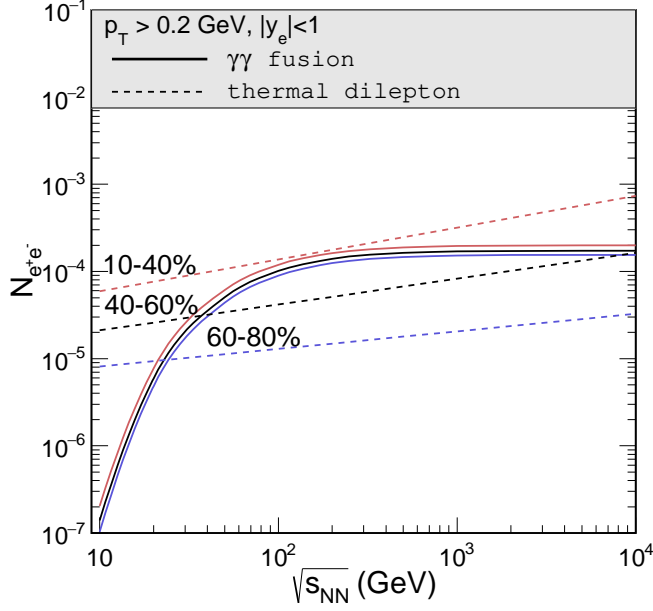


FIG. 4: Excitation function of low- P_T (<0.15 GeV) dilepton yields from $\gamma\gamma$ fusion (solid lines) and thermal radiation (dashed lines) in collisions of heavy nuclei ($A \simeq 200$) around midrapidity in three centrality classes, including single- e^\pm acceptance cuts.

so again in the TeV energy range for more central collisions. On the other hand, the $\gamma\gamma$ fusion contribution is most significant around the regime where it levels off, where its yield is (much) larger than the one from thermal radiation for semi-/peripheral collisions, and comparable for semi-central collisions. Our analysis therefore identifies the RHIC energy regime as the most promising ground to investigate this production mechanism.

IV. CONCLUSIONS

We have studied low- P_T dilepton production in ultrarelativistic heavy-ion collisions, by conducting systematic comparisons of the two sources that are believed to be prevalent in this regime, *i.e.*, thermal radiation and photon-photon fusion within the coherent fields of the incoming nuclei. The former was taken from a well-tested model including in-medium hadronic and QGP emission rates, while the latter was calculated utilizing photon fluxes with realistic nuclear form factors including the case of nuclear overlap. We first reconfirmed the finding of a recent STAR analysis that the combination of the two sources (augmented by a contribution from the hadronic final-state decay cocktail) gives a fair description of low- P_T dilepton data in Au-Au ($\sqrt{s_{NN}}=200$ GeV) collisions in three centrality classes for invariant masses from threshold to 4 GeV (with the exception of the J/ψ peak, indicating an additional production mechanism not included here). The coherent emission was found to be dominant for the two peripheral samples, and comparable to the cocktail and thermal radiation yields in semi-central collisions.

At the lower SPS energies ($\sqrt{s_{NN}}=17.3$ GeV) we found that the $\gamma\gamma$ contribution is sub-leading. Specifically, for acceptance-corrected low- P_T dimuon spectra as measured by NA60 in MB In-In collisions, it reaches up to ten percent of the thermal radiation for

masses near the dimuon threshold, rapidly falling off with increasing mass. On the other hand, at the high-energy frontier, the situation turned out to be similar to RHIC energies, although the role of thermal radiation relative to the coherent mechanism is somewhat more pronounced in the multiple-TeV range. The interplay of these processes at the LHC is of particular interest in view of plans by ALICE [36] to lower the single-electron p_T cuts and measure very-low mass spectra to possibly extract the EM conductivity from thermal emission.

We have summarized our results in an excitation function of low- P_T radiation covering three orders of magnitude in collision energy. While coherent production increases rather sharply, and then levels off, near $\sqrt{s_{NN}} \simeq 100$ GeV, thermal radiation increases more gradually with s_{NN} . This explains why the latter is dominant at the SPS, the former dominates at RHIC, and the latter becomes more important again at the LHC.

Acknowledgments

This work has been supported by the US National Science Foundation under grant no. PHY-1614484 (RR) and by the Polish National Science Center grant DEC-2014/15/B/ST2/02528 (MKG, WS, AS).

-
- [1] E. L. Feinberg, *Nuovo Cim. A* **34** (1976) 391.
 - [2] E. V. Shuryak, *Phys. Lett. B* **78** (1978) 150.
 - [3] I. Tserruya, in *Relativistic Heavy-Ion Physics*, edited by R. Stock and Landolt Börnstein (Springer), New Series **I/23A** (2010) 4-2 [arXiv:0903.0415[nucl-ex]].
 - [4] H.J. Specht [for the NA60 Collaboration], *AIP Conf. Proc.* **1322** (2010) 1.
 - [5] R. Rapp, G. Chanfray and J. Wambach, *Nucl. Phys.* **A617** (1997) 472.
 - [6] P. M. Hohler and R. Rapp, *Phys. Lett. B* **731** (2014) 103.
 - [7] R. Rapp and E. V. Shuryak, *Phys. Lett. B* **473** (2000) 13.
 - [8] J. Ruppert, C. Gale, T. Renk, P. Lichard and J. I. Kapusta, *Phys. Rev. Lett.* **100** (2008) 162301.
 - [9] R. Rapp and H. van Hees, *Phys. Lett. B* **753** (2016) 586.
 - [10] S. Afanasiev *et al.* [PHENIX Collaboration], *Phys. Lett.* **B679** (2009) 321.
 - [11] E.L. Kryshen for the collaboration [ALICE Collaboration], *Nucl. Phys.* **A967** (2017) 273.
 - [12] ATLAS Collaboration, ATLAS-CONF-2016-025.
 - [13] A. van Hameren, M. Klusek-Gawenda and A. Szczurek *Phys. Lett.* **B776** (2018) 84.
 - [14] M. Klusek-Gawenda and A. Szczurek, *Phys. Rev. C* **93** (2016) 044912.
 - [15] J. Adam *et al.* [ALICE Collaboration] *Phys. Rev. Lett.* **116** (2016) 222301.
 - [16] W. Shi, W. Zha and B. Chen, *Phys. Lett.* **B777** (2018) 399.
 - [17] J. Adam *et al.* [STAR Collaboration], arXiv:1806.02295 [hep-ex].
 - [18] S. R. Klein, *Phys. Rev. C* **97** (2018) 054903.
 - [19] W. Zha, L. Ruan, Z. Tang, Z. Xu and S. Yang, *Phys. Lett. B* **781** (2018) 182.
 - [20] T. Song, W. Cassing, P. Moreau and E. Bratkovskaya, arXiv:1806.09377 [nucl-th].
 - [21] R. Arnaldi *et al.* [NA60 Collaboration], *Eur. Phys. J. C* **61** (2009) 711.
 - [22] C. A. Bertulani and G. Baur, *Phys. Rept.* **163** (1988) 299.
 - [23] G. Baur, K. Hencken, D. Trautmann, S. Sadovsky and Y. Kharlov, *Phys. Rept.* **364** (2002) 359.
 - [24] H. De Vries, C. W. De Jager and C. De Vries, *Atom. Data Nucl. Data Tabl.* **36** (1987) 495.

- [25] E. Shuryak, Prog. Part. Nucl. Phys. **62** (2009) 48.
- [26] U. Heinz and R. Snellings, Ann. Rev. Nucl. Part. Sci. **63** (2013) 123.
- [27] C. Gale, S. Jeon and B. Schenke, Int. J. Mod. Phys. A **28** (2013) 1340011.
- [28] R. Rapp, Adv. High Energy Phys. **2013** (2013) 148253.
- [29] M. Urban, M. Buballa, R. Rapp and J. Wambach, Nucl. Phys. A **673** (2000) 357.
- [30] T. Galatyuk [HADES Collaboration], Nucl. Phys. A **967** (2017) 680.
- [31] G. Agakichiev *et al.* [CERES Collaboration], Eur. Phys. J. C **41** (2005) 475.
- [32] P. Huck [STAR Collaboration], Nucl. Phys. A **931** (2014) 659.
- [33] L. Adamczyk *et al.* [STAR Collaboration], Phys. Rev. C **92** (2015) 024912.
- [34] A. Adare *et al.* [PHENIX Collaboration], Phys. Rev. C **93** (2016) 014904.
- [35] S. Basu, T. K. Nayak and K. Datta, Phys. Rev. C **93** (2016) 064902.
- [36] F. Antinori, P. Braun-Munzinger and S. Flörchinger, priv. comm. (2018).